Low noise, dual gain preamplifier with built in spectroscopic pulser for highly segmented high-purity germanium detectors

G. PASCOVICI (1), A. PULLIA (2), F. ZOCCA(2), B. BRUYNEEL (1), D. BAZZACCO (3)
(1) Institute of Nuclear Physics, University of Cologne, Germany
(2) University of Milan, Department of Physics and INFN-Sezione di Milano, Italy
(3) INFN-Sezione di Padova, Italy
G.Pascovici@ikp.uni-koeln.de

We present a fast and very low noise hybrid front-end electronic device consisting of a complex charge sensitive preamplifier with a built in fast reset circuitry and a very accurate spectroscopy pulser. The front-end electronics was developed for the central electrode of 36-fold segmented, high purity germanium detectors in the frame of AGATA array of detectors. The intrinsic energy resolution in conjunction with a highly segmented detector is less then 900 eV for central electrode with a detector capacity of ~ 47 pF. The dynamic range of the central charge sensitive stage is as large as 100 dB, ranging from 0.1 fC to 10 pC, i.e. from ~2 keV to 180 MeV in terms of photon energy. To achieve such an unprecedented wide dynamic range, we split the whole spectroscopic range in four sub-ranges, namely 0-5 MeV, 0-20 MeV, 5-180 MeV and 20-180MeV, respectively. The first two ranges are measured with standard pulse-high spectroscopy techniques. Thereto, the analog electronics was designed with two conversions gains, 200 mV/MeV and 50mV/MeV, respectively to match the 1 V input dynamic range of the very fast pipe line ADC used by the digitizer units. To extend the pulse-height spectroscopy range well beyond the fast ADC analog input range, a new method was implemented and at a certain threshold we are switching from a standard pulse height analysis method to a time over threshold technique [TOT]. In order to achieve that, adjacently to the pole-zero cancellation circuit, a fast-reset circuit controlled by a fast comparator and an accurate zero crossing detector has been developed. Using this technique we can achieve an energy resolution of 0.04% at equivalent gamma energies of 180MeV. A programmable spectroscopic pulser has been designed and implemented in the central electrode (core) front-end electronic to achieve 'self-calibration standards' in both time and amplitude domain, which was needed to characterize such a complex, highly segmented high purity solid state detector.

Key-Words: - low noise, fast preamplifier, tracking gamma spectroscopy, extended ADC range

1 Introduction

The "Advanced Gamma Tracking Array" AGATA [1] will be a device of major importance for nuclear structure studies at the very limits of nuclear stability, capable of measuring gamma radiation in a large energy range (from a few tenths of keV up to more then 10 MeV) with greatest possible efficiency and very good spectral response. With the advantage of the first genera-tion of radioactive beam facilities dedicated medium size detector arrays (e.g. Miniball [2] and Exogam [3]) the AGATA gamma-ray spectroscopy instrument (Fig.1) is based on a new concept and technique of gamma-ray energy tracking in electrically segmented high purity Ge crystals. The realization of such a system required the develop-ment of highly-segmented Ge detectors, digital electronics, pulse shape analysis (PSA) to extract energy, time and position information and tracking algorithms to reconstruct the full interaction. One of the key issues in the whole system design is the development of accurate front-end electronics with

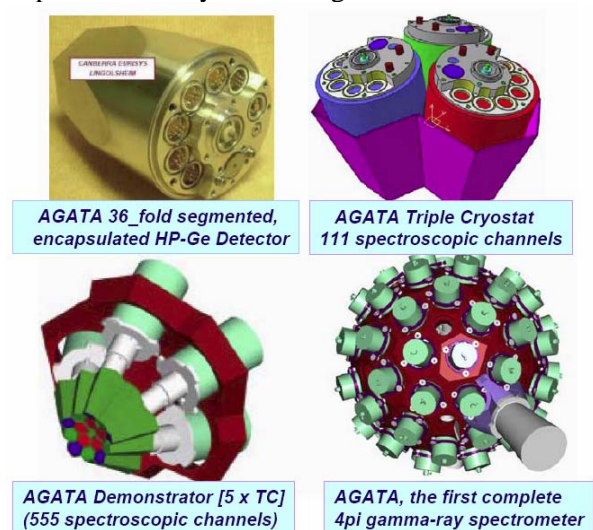clean transfer function at high counting rate and unprecedented dynamic range.

Fig.1 An overview of the AGATA detector, AGATA-Triple, AGATA demonstrator and full AGATA array, -the first complete 4π gamma-ray spectrometer

G. Pascovici, A. Pullia, F. Zocca,
B. Bruyneel, D. Bazzacco

Indeed, the use of pulse-shape analysis technique raises an additional issue to the preamplifier specification, namely a fast rise time (faster than the fastest collection time of electrons and holes in a detector) and moreover a very clean transfer function in the time domain, good behavior at high counting rates and unprecedented dynamic range. The good transfer function has to be preserved in cryostats equipped with multiple highly segmented detectors and with their real internal wiring. The crosstalk between channels has to be as small as possible (by design it is in the order of magnitude of ~ 10^{-3} or less).

A very large dynamic range at high counting rates is mandatory, to detect gamma-rays alone in the range up to 10-20 MeV and additionally in the presence of pile-up effects induced by some energetic charged particles, e.g. pions and kaons. Some of those charged particles can generate signals in the HP-Ge detector with very high amplitudes, equivalent to gamma energies of 50-100MeV. Special care has to be taken in the design of the front-end analog electronics to avoid saturation due to pile-up effects of those signals above 10 kcps.

We have developed a dedicated front-end electronics device for the central contact (core) of a highly segmented HP-Ge detector consisting of a charge-sensitive preamplifier and a programmable spectroscopic pulser circuitry (Fig.2). To reduce substantially the dead time caused by large signals or piled-up of large signals and to avoid the saturation of the output buffer, the preamplifier is equipped with a time-variant device which quickly resets the large signals above a threshold. The threshold is put just below the upper limit of the ADC input range and it will be shown how this device reduces the dead time induced by large signals by a large factor of 4 to 5 and how it additionally it extends the pulse-height measurement range well beyond the ADC linear range using the TOT technique.

2 Front-End Electronics Structure

As shown in Fig.2, the structure of the front-end electronics consists of the following stages: a charge-sensitive loop including a part cooled at about 150 K, a pole-zero cancellation with integrated fast reset circuitry, a balanced differential output buffer and a programmable spectroscopic pulser unit. The warm part is built in two versions, one as "single core" (100mV/MeV) and another one as "dual core" with two gains, namely 200mV / MeV and 50 mV / MeV, respectively.
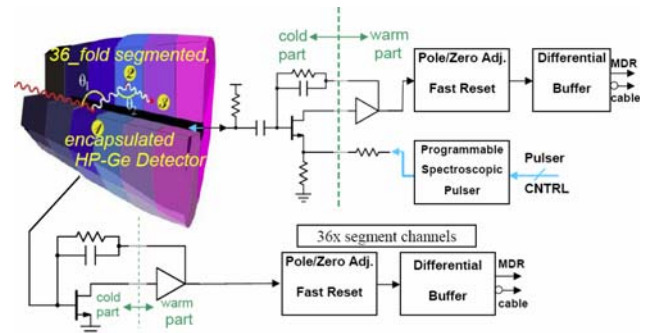

Fig.2 AGATA Analog front-end electronics for the central contact (single core version) and for the 36 segments

2.1 Charge-Sensitive Loop

The input stage is collecting electrons from the central electrode of a 36-fold segmented detector. The connection is AC (1nF/5kV) due to a 4-5 kV bias voltage applied to this electrode. The charge-sensitive cooled part comprises an input stage with a very low noise jFET transistor and a passive feedback network. These components are placed in a cryostat near the central electrode to reduce the noise and the microphonic effects. A temperature between 150 K +/- 25 K was chosen for the input jFET in order to optimize its equivalent noise voltage down to ~ 0.6 nV/$\sqrt{Hz}$ [3]. The feedback network time constant of the first stage is 1 ms (1GOhm and 1pF, respectively) to optimize both noise and bandwidth in the first stage. The Transimpedance Amplifier (TA) designed with discrete components is operated at room temperature outside the cryostat. A 'folded cascode' structure was adopted for the TA stage (Fig.3). The TA is optimized for a wide unipolar output range of ~10V positive swings, with the unusual solution of two cascaded bipolar transistors in the common-base path (Q1; Q3). This was a convenient solution with the advantage of increased open-loop gain of the charge-sensitive stage balanced by the small disadvantage of increased noise of the double transistor cascode structure. By properly biasing the circuit structure, the increase in noise due to the double transistor cascade structure was rendered negligible. As the closed-loop gain is 53 mV/MeV (for $C_F = 1$ pF) and the output voltage range of the TA stage is about 10 V, we obtain an energy range of 180MeV with an intrinsic noise of 600eV @150K and with a slope of 8eV/pF (with a total detector bulk capacity of ~ 47pF). To get a fast rise time at lowest possible noise, several jFET structures have been tested e.g. IF1320 (InterFET), BF861A, -B, -C, BF862 (Philips). The BF862 was finally selected.

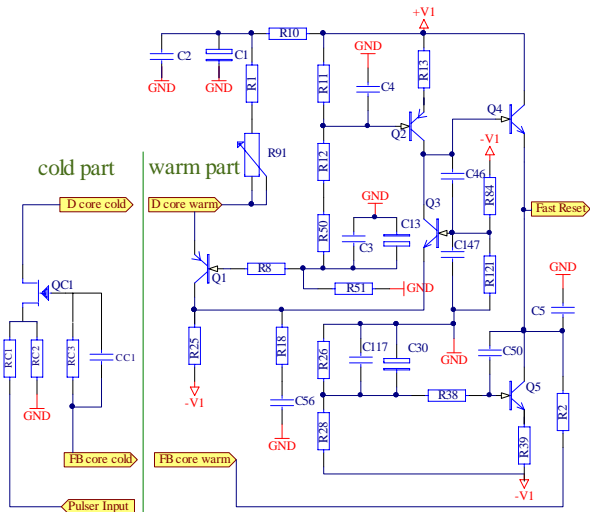G. Pascovici, A. Pullia, F. Zocca,
B. Bruyneel, D. Bazzacco

Fig.3 Core- preamplifier charge-sensitive loop (left, cold part and right, warm part -TA stage)

We also optimized the double transistors cascode circuitry for a low noise and a wide bandwidth by carefully choosing the collector currents Q1 and Q3 to an optimum value of 450 µA.

2.2 Pole-Zero cancellation with integrated Fast Reset circuitry

The second stage of the preamplifier section is a passive Pole-Zero cancellation (P/Z Adj.) network and a buffer stage as impedance matcher. The P/Z Adj. stage has the purpose of reducing the decay time of the first charge-sensitive stage (of 1000 µs) down to 50 µs. Therefore, the baseline restoration is faster and the event-by-event pile-up is reduced. The P/Z Adj. works properly up to 20-30 kcps and mean energies around 1-2 MeV. Unfortunately, this adjustment is less efficient at much higher counting rates in combination with high energetic background of much higher pulses, up to 50-100 MeV equivalent gamma energies. To speed up the baseline restoration in such cases, we implemented a fast time-invariant reset circuitry. It consists of an accurate fast trigger comparator which switches on/off a temperature-compensated current sink, placed behind the passive P/Z Adj. circuit (Fig.4). When a large signal arrives, the current sink is switched on, which discharges the capacitance $C_{P/Z}$ which quickly restores the output voltage to 0 V. As soon as the voltage $y(t)$ reaches 0V, the current sink is switched off and normal operation is restored. As shown in Fig.4 and Fig.5, an ultra fast comparator is continuously sensing the preamplifier output signal. The LT1719 with less than 6ns output/input delay at only 5mV input overdrive has been chosen for this purpose. The control of the fast reset device is made statically or dynamically through a single wire called SHDN. One can

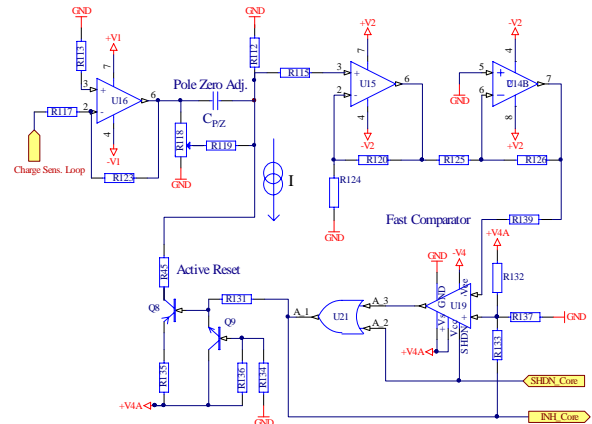handle the SHDN statically keeping it permanently up or down or dynamically.

Fig.4 Fast Reset current sink circuit through Pole-Zero network

F. Zocca [6] calculated exactly the relation between the width of the inhibit signal (T) and the amplitude of a very large signal, over the comparator threshold.
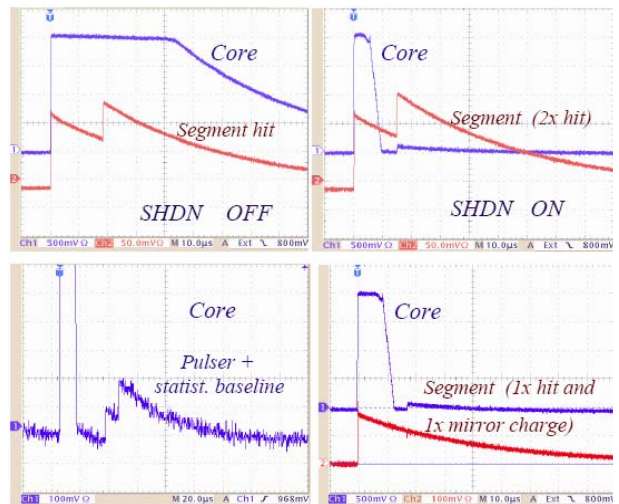

Fig.5 Time diagram of the time-variant fast reset circuit (left above, SHDN OFF, right above and below, SHDN ON) and Fast Recovery <2µs after INH signal (left below, expanded baseline).

It turned out that after measuring $T = t_2 - t_1$ (Fig.6) we can estimate the energy of the large signal as:

$$E_w = b_1T + b_2T^2 - E_c \qquad (1)$$

Where b_1 and b_2 are parameters independent of T and the E_c is the exponential tail, namely:

$$E_c = E_1 - E_2 + E_o \qquad (2)$$

Where E_1 and E_2 are the averaged pre- and post-pulse baseline estimates (V_1, V_2) expressed as energy values and E_o is an offset term.
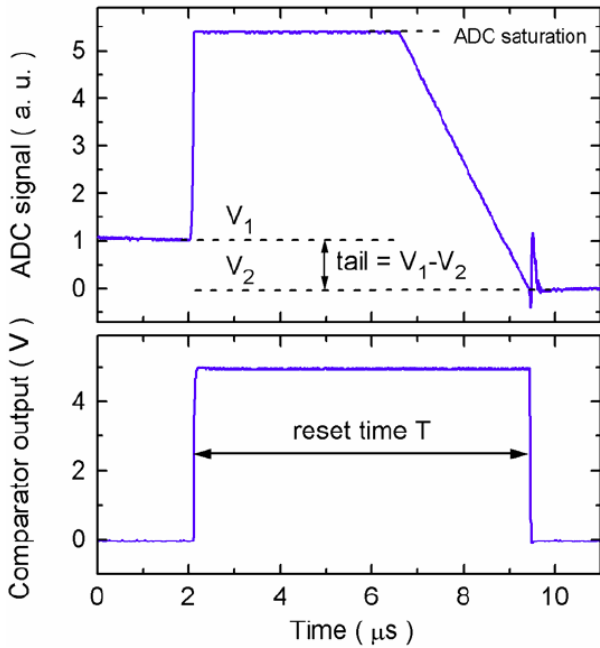

Fig.6 Measurement technique of time over-threshold technique

The final expression for the large signal energy as function of the reset time and pre- and post-pulse voltage baseline (V_1 and V_2) is given by:

$$E_W \cong b_1 T + b_2 T^2 - \frac{V_1 - V_2}{G} + E_0 \qquad (3)$$

where

$$b_1 = \psi \frac{I}{q} \frac{C_F}{C} \quad \text{and} \quad b_2 = \frac{b_1}{2\tau_P} \qquad (4)$$

Unfortunately, while C_F and C are not calibrated we can hardly calculate parameters b_1 and b_2, but we can take advantage of an existing spectroscopic pulser on board and fix b_1 and b_2 using large precise pulser signals of different pre-calibrated and over-threshold equivalent energies. Additionally, if we simultaneously irradiate the detector with gamma-rays, with energies well below the threshold, then we can also generate a statistical distribution of the disturbing tails as shown in Fig.5 (left, bellow). The equation (3) establishes a linear relation between the measured data and the parameters b_1, b_2, E_o, thus we can extract those parameters from three or more experimental points. We need to generate different values for T, each with different pulser amplitudes above the threshold. Following this procedure energy

resolution better than 0.02% can be obtained at 100MeV equivalent gamma energies.

2.3 The differential balanced output buffer

A differential signal transmission mode was selected to enhance the rejection to common-mode noise and disturbances picked up along the output cable. As output stage, a balanced differential output stage has been designed around LM6172 dual operational amplifier which features low noise, low power and wide bandwidth (Fig.7). Only +/- 6V power supplies have been chosen due to the overall power consumption limitation of the triple cryostat, holding 111 spectroscopic channels of three AGATA detectors (3x36 segment channels and 3x core channels).
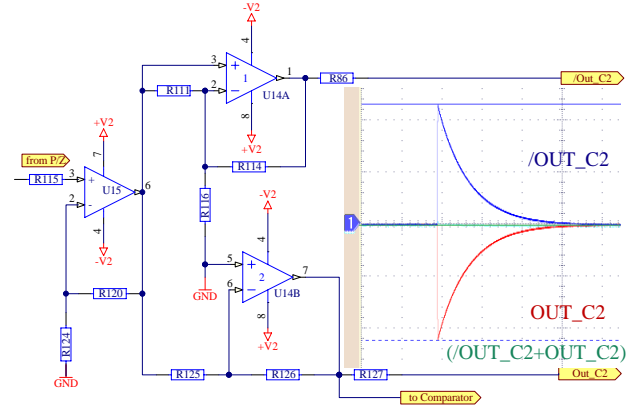

Fig.7 Balanced differential buffer and twisted cable driver circuit

The signals are transmitted to the remote ADC modules through 10 m individually shielded twisted pair cables preserving the original quality of the signals, which makes the preamplifier assembly suitable for noisy experimental environments. A high quality 26-wire LVDS cable assembly with 11 individually shielded twisted pairs ("camera-link" like format) and MDR (Mini Delta Ribbon) male connectors on either side have been chosen.

2.4 Programmable spectroscopic pulser

One of the important issues in the framework of the AGATA detector and triple cryostat development is the characterization of its response function, including the response function of the preamplifiers (both in time and frequency domains), e.g. stability, linearity, treatment of saturated pulses, dependency of the energy resolution on counting rate, dead time estimation, microphonics effects of the detector and cryostat, intrinsic detector characterization (bulk capacities) etc. Many of these parameters can be measured with the help of a high precision spectroscopic

G. Pascovici, A. Pullia, F. Zocca,
B. Bruyneel, D. Bazzacco

pulser and this is the main reason why a Programmable Spectroscopic Pulser (PSP) has been developed. It is used for detector characterization and also for the self calibration [11] of the TOT method.

The output signal of the PSP is DC coupled to the source pin of the core jFET through a resistor divider consisting of a $48.5\,\Omega$ resistor and a grounded $1.8\,\Omega$ resistor. Thereafter, the signal reaches each of the 36 detector segments via the source-gate capacitance of the jFET, the HV coupling capacitor and the core-segment bulk capacitance (Fig.2). A block diagram of the PSP is showing in Fig.8 and the main specifications are presented in Table 1.

The PSP consists of three stages: a programmable reference voltage (V_{Ref}), a chopper, triggered by an external signal (*Pulser In*) and a programmable attenuator which comprises also an output buffer stage (*Programmable Attenuator-Buffer*).
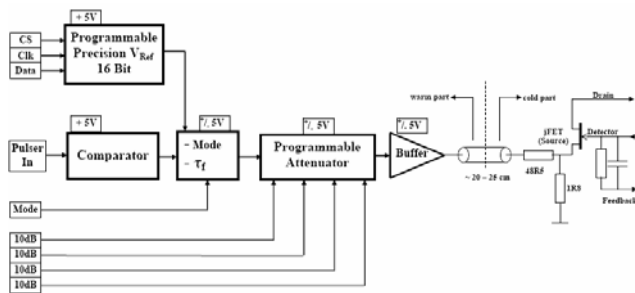

Fig.8 Block diagram of the Programmable Spectroscopic Pulser

Table 1 Specification for spectroscopic pulser

Property		Value	
Dynamic range core	[MeV]	0.05-150	
ditto segments	[MeV]	0.005- 3	
Resolution core	[keV]	< 1.15	
Resolution segments	[keV]	< 0.9	
Rise time (default)	[ns]	50	(opt.20-80)
Fall time (default]	[μs]	150	(opt. 1000)
Stability: long term		~$1.2.10^{-4}$ / 24h	
Stability: temperature		~ 2.5 ppm / ^{o}C	

The programmable reference is built around an ultra high precision voltage reference of 4.096 V (MAX6341ESA) with a very low temperature coefficient (1 ppm/ °C), very low noise (1.5 μV pk-pk), long-term stability of 30 ppm/1000 hr and a 16 bit serial input, voltage DAC (+/- 1bit), type AD5541CR. Data is written to it in a 16-bit word format, via a 3-wire industry standard serial interface with CS, Clock and Data In signals. The output of the programmable reference stage is a

low noise and very fast rail-to-rail operational amplifier (OPA354) with relatively large slew rates in both directions, being able to source and sink fast chopped currents.

The Chopper is built around two ADG751 analog switches. It is designed in a T-switch configuration, which results in excellent Off Isolation while maintaining good frequency response in the ON condition. The chopper stage is triggered by an external signal (Fig.9). A balanced differential transmission (LVDS type) has been adopted for this signal to reduce its crosstalk with the analog signals.

The chopper mode of operation is programmable; a rectangular or an exponential-decay mode can be selected. In exponential mode the decay time is set by default to 150 μs but it is adjustable in the range of 50 μs up to 1000 μs. If the exponential-decay mode was selected, a linear gate circuitry selects only the positive polarity.
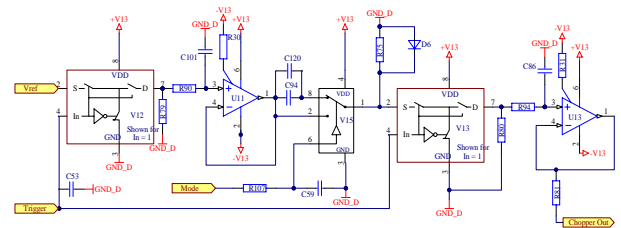

Fig.9 Spectroscopic pulser, chopper and linear gate

The last stage is a programmable attenuator, which consists of four stages, each of 10dB; thus the coarse attenuation factor can be selected between 0 and 40 dB, with a granularity of 10 dB. The buffer stage (LT1815) can drive a maximum DC current of 20 mA onto a tiny load resistor with a nominal value of $1.8\,\Omega$, placed in the cryostat between the source pin of the core jFET and internal GND (Fig.8).

2.5 Dual Gain Core Structure

From the discussion of the TOT method, presented in the subsection 3.2, it is evident that a small "open gap" in signal amplitude range remains between the classical amplitude spectroscopy method and the Time-Over-Threshold method.

Analogous to the subranging ADC methods, where some extra bits are used in the extra stages to correct the errors made in earlier stages, it was decided to build a new version of the AGATA Core Preamplifier, namely one board with two conversion gains.

The previous AGATA Single Core board had only one conversion range of ~100mV/MeV, switching from the classical amplitude mode to the TOT method at about 10MeV.

G. Pascovici, A. Pullia, F. Zocca,
B. Bruyneel, D. Bazzacco

The Dual Core preamplifier has one channel with larger conversion gain range of ~ 200 mV/MeV and another one with only ~ 50 mV/MeV.

The advantage of a board with dual channel gains is at least twofold. Firstly the channel with higher gain will be able to analyze the smaller range of spectra with higher accuracy (and in normal applications this part of the spectra has higher incidence rate).
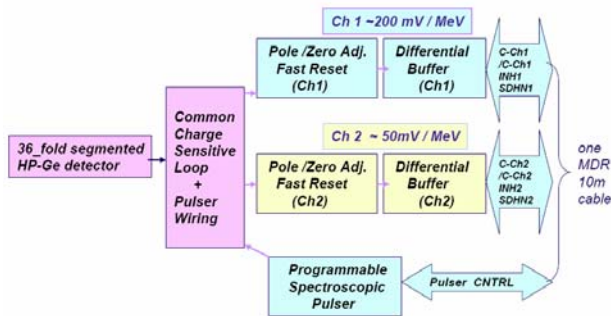

Fig.10a The block diagram of the dual core with Programmable Spectroscopic Pulser
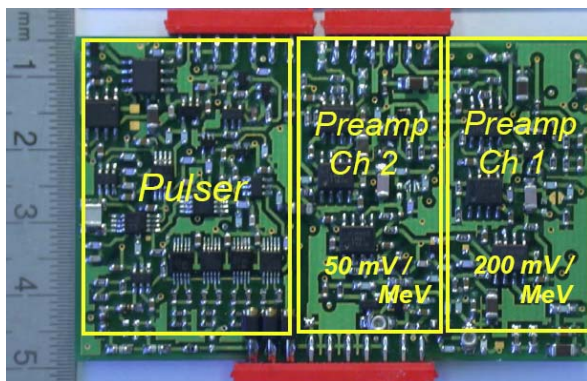

Fig.10b Dual gain core preamplifier and program-mable spectroscopic pulser (top view)

Therefore the first channels switches to the TOT method at about 5 MeV, while the second channel will switch to the TOT method at about 20 MeV. In this way, the second channel will cover the narrow subranging "open-gap" of the first channel, being at about 5MeV in its full linear range and therefore can be used to correct the first channel.

To preserve the good transfer function of all preamplifiers special attention has been paid to the cryostat wiring, especially to the return ground paths. The structure of the dual core preamplifier is shown in Fig. 10a. The layout of the dual gain core preamplifier and programmable spectroscopic pulser is displayed in Fig.10b.

Almost ideal transfer functions in time domain for pulser amplitude of equivalent ~19 MeV are presented in Fig. 11 for the two core channels Ch1, Ch2 and for one of the segment.
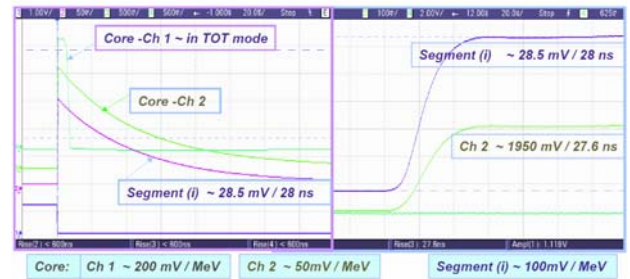

Fig.11 The transfer functions in time domain for the dual gain core channels and one of the segments at ~19 MeV equivalent input gamma energy.

The first core channel (Ch.1) is in TOT mode of operation and the second core channel (Ch.2) and all segments are in linear mode of operation.

3 Measurements with dual core pre-amplifier and spectroscopic pulser

The amplitude resolution was tested in a setup with a test cryostat (with 47pF as segmented "dummy" detector), an Ortec Filter Amplifier with 6µs shaping time (Model No.671A) and a 16k channels IKP MCA [4]. In this setup we obtained for the spectroscopic pulser an equivalent energy resolution of ~1keV FWHM for the core Ch.1, of about ~1.1keV FWHM for core Ch.2 and ~0.9keV FWHM as mean value for all the segment channels, i.e. the equivalent intrinsic energy resolution of the spectroscopic pulser is less then ~0.6keV FWHM.
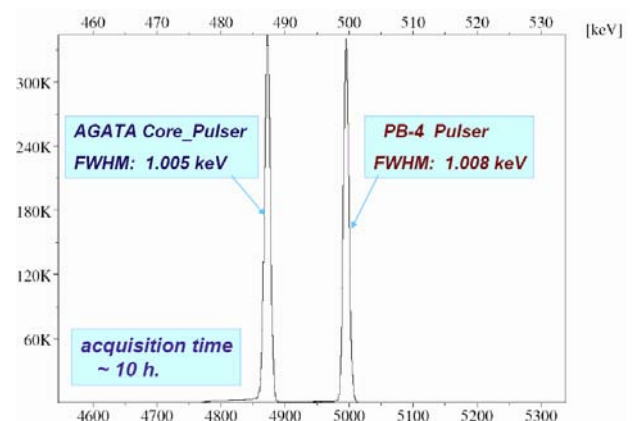

Fig.12 Energy resolution of AGATA Core-PSP vs. PB-4 (BNC) spectroscopic pulser

In a second setup, the preamp was tested in this AGATA test cryostat in conjunction with a real

symmetric 36-fold segmented AGATA detector, biased at 4kV.

A full set of core-pulser and segment preamplifier boards were installed in the cold part as well as in the warm part of the detector cryostat. As mentioned before, all jFETs (36 for the segments plus one for the core) and all feedback passive components (namely, the 1GΩ and 1pF) were placed in the cryostat and cooled down with liquid nitrogen to about 150K, while the detector is cooled down very close to the liquid nitrogen temperature.

Table 2 Full specifications of the AGATA Single and Dual Core Preamplifiers

Property	Value	Tolerance
Conversion gain for segments and single core	100 mV / MeV (terminated)	±10 mV
Conversion gain for dual core	200 mV/MeV (Ch 1) 50 mV/MeV (Ch 2)	±20 mV ±5 mV
Noise	0.6 keV FWHM (C_d=0 pF @ 150K)	
Noise slope	+ 8 eV / pF	±2 eV
Rise time	~13 ns (0 pF)	±2 ns
Rise-time slope	~0.2 ns / pF	
Decay time	50 µs	±2 µs
Integral non linearity	< 0.025% (Dyn.~3.5V)	
Output polarity	Differential, Z_o=100Ω	
Fast reset speed	10 MeV/µs Single Core	
Inhibit output	LVDS (EIA/TIA-644)	
Power supply	± 6.5 V, ± 12.5 V	±0.5V
Power consumption jFET	< 20 mW	
Power consumption (except diff. buffer)	< 350 mW Single Core (<600 mW Dual Core)	
Supplementary power at very high counting rates	~230 mW Single Core (~460 mW Dual Core)	
Mechanical dimension	62 x 45 x 8 mm Single (70 x 50 x 7mm Dual)	

In this setup, the mean energy resolution observed in the core spectra on the 1.33 MeV line of ^{60}Co was 2.19 keV FWHM and about 1.1-1.2 keV FWHM on the 122 keV/136 keV ^{57}Co lines.

One of the acquired spectra is shown in Fig.13 and expanded very the low energies part and high energies part, respectively. The pulser pulse height amplitude has been programmed for both regions of interest, in a sequential mode of operation, namely at equivalent ~1250 keV (high energy) and ~60 keV (low energy), respectively.
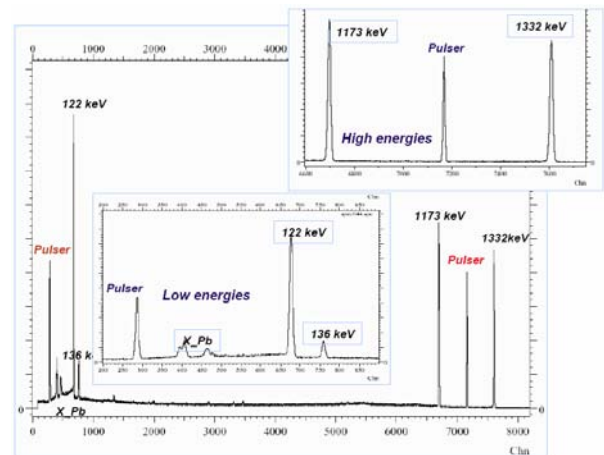

Fig.13 Acquired core spectra with low energy gamma-ray lines and intercalated pulser lines

3.1 Detector electrical characterization

Taking advantage of the built-in pulse generator in the AGATA Core Preamplifiers one can measure directly some intrinsic detector parameters, not specified by the detector manufacturer, but very useful in data treatment and interpretation. One of these parameters is the bulk capacity between the central electrode (core) and individual segments. The pulser signal is injected in the source of the core jFET and distributed over all detector segments by its central contact as presented in subsection 2.4 and Fig.19. The pulser signal amplitude, measured in each segment will be inversely proportional to the core-to-segment bulk capacity which acts as coupling capacity. Since the preamplifiers are not calibrated in absolute sense, the core-to-segment bulk capacity measurements only provides relative data but these values can be calibrated with the total detector capacity, i.e. their sum should be equal to the whole detector bulk capacity.

Table 3 Mean values for ring bulk capacities

Ring number	1	2	3	4	5	6
Mean segment capacity [pF]	1.20	0.84	1.22	1.53	1.45	1.55

For example, in the case of the first symmetric 36-fold segmented AGATA detector (S001), the detector manufacturer guaranteed a total bulk capacity of 46.7pF. From the pulser core-segment amplitude ratios the bulk capacities of the segments could be measured, normalizing them to a total bulk capacity of 46.7pF. The mean values for segment capacities are presented in Tab.3 (there are 6 rings each segmented in 6 sectors).
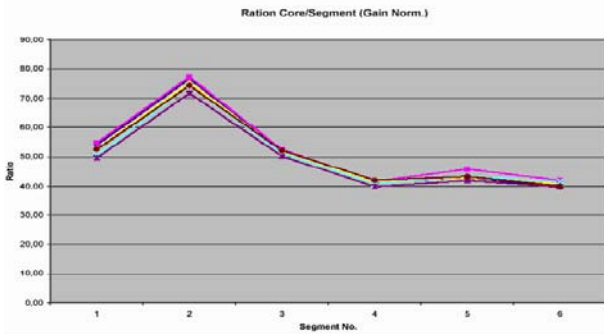
Fig.14 Experimental Pulser Core/Segment ratios for one of the AGATA symmetric detectors (S001)

Due to the symmetry of this detector, these capacities are only ring dependent. The deviations of the measured values with the listed averages for segments within the same ring coincide within a standard deviation of 3.5%. These capacities play a leading role in the propagation of cross talk (see section 3.3).

3.2 Time Over Threshold (TOT) technique from 5 MeV to 180 MeV

The spectroscopic pulser resolution measured in normal spectroscopic mode is between 1.05 keV and 1.15 keV FWHM in relative wide range of equivalent energies, from 50keV up to 3 MeV. Tested in conjunction with the TOT technique and in the presence of a background of regular statistical signals from a calibration radioactive source (such as ^{60}Co) the resolution is better than 0.4% over the full range and better than 0.04% between 50-150 MeV, as shown in Table 4.

The TOT technique has been tested in a setup with real high energetic γ-rays produced by an ^{241}Am+Be source with a Ni target generating high-energy photons by neutron capture reactions [5]. In this experimental setup the reset threshold was intentionally set to a lower value of ~3MeV, in order to reserve a large part of the whole spectrum of the ^{241}Am+Be γ-ray spectrum in the "reset mode" (i.e. TOT technique).

In Fig. 15 (above) a high energy spectrum of a ^{241}Am+Be radioactive source is shown as acquired beyond the ADC range with our front-end electronics working in the Wilkinson mode (TOT technique). The energy of the events is derived from the reset time through relation (3). The part of the spectrum at energies < 3 MeV has been also acquired in normal pulse-height mode but is not shown here. For comparison we also show in Fig.15 (below) the same spectrum as acquired in amplitude mode only, after reducing the electronic-chain gain in such a way that the ADC range reached 9.4 MeV.
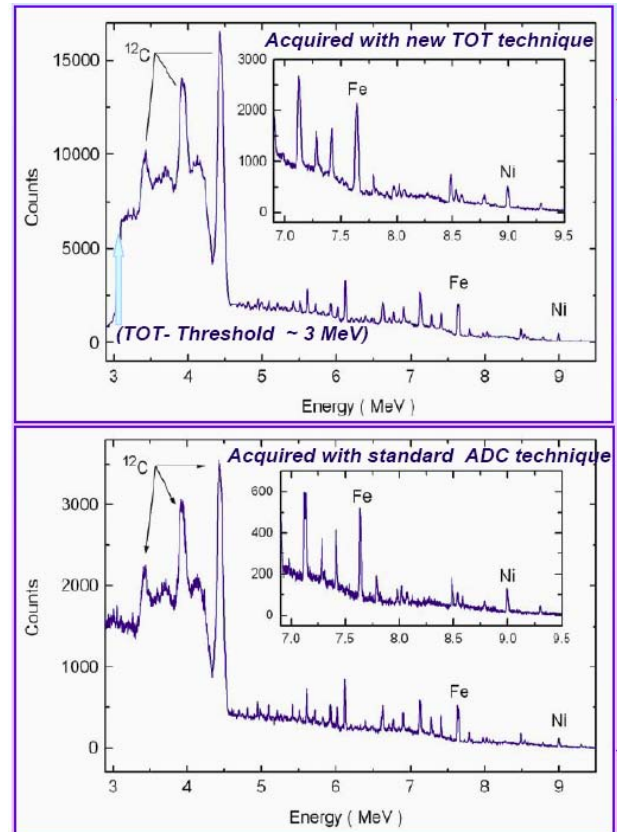

Fig.15 Acquired high energy spectra with γ-rays of an ^{241}Am+Be radioactive source as obtained with two different methods: above with TOT technique and below with the normal spectroscopy technique

Note that gain reduction yielded a worsening of ~0.2 keV FWHM in the energy resolution, caused by the higher impact of second-stage and pick-up noises. The excellent correspondence of the two spectra however is evident, which proves the effectiveness of the Wilkinson-mode measurement technique. Using a high-precision pulser to simulate large detector signals we could then verify that the range of the measurements in Wilkinson mode reached 180MeV of equivalent energy.

Table 4 Pulser resolution at low counting rates:

Pulser Amplitude, Equiv. energy [MeV]	3.5	6.0	10.0	20.0	30.0	50.0
Pulser resolution [%]	.35	.19	.11	.07	.045	.039

Increasing the counting rates from 800cps up to 15kcps the pulser resolution is still very good, i.e. better than 0.21% for all tested counting rates and feeding in equivalent energies of 6, 10 or 20 MeV.

3.3 Low frequency transfer function

In such a complex detector system where the sensor itself is highly segmented, cross talk between segments is observed between core and segments and vice versa. Special care has been taken to minimize the cross talk between segments, between core and segments and between detectors at the level of the triple cryostat. The cold jFET PCBs have been carefully designed to minimize the inductive coupling between neighboring segments channels, also an additional number of return ground wires for the segment grounds wiring in the cryostat have been added. In the case of the triple cryostat to avoid additional crosstalk between detectors, separated return ground paths for the three central detector contacts and for the core-pulser signals have been provided.

In order to minimize the parasitic capacitors and inductivities, the cold part (Fig.3) is placed near the detector capsule and in this way the stray capacities are less then 0.2 pF and the inductivities less then 10nH for each electrode. However, the use of encapsulated detectors makes that the inductivities to the segment electrode within the encapsulation cannot be omitted. The important consequence of this will be demonstrated further.

In E. Gatti et al [6] and E. Pellegrini et al. [7], a realistic AC equivalent detector model was presented. It extends the Shockley-Ramo theorem by taking into account the capacities between segments (table 3). This causes that the charge signals created at the electrodes of a real segmented detector are coupled to each other according to:

$$i_i = i_i^{Ramo} - \sum_{j \neq i} C_{i,j} \frac{\partial V_j}{\partial t} \qquad (5)$$

with i^{Ramo} the currents as calculated by the Shockley-Ramo theorem, $C_{i,j}$ the capacity between segment or core electrodes i and j and V_j, the potential at electrode j. It has already been demonstrated [9] that this extension is at the origin of the highly periodic cross talk observed in the AGATA detector segments, fig 17. The transfer function at low frequencies can be described by:

$$i_{Ramo} = \mathbf{Z}(f < 1\text{Mhz})\, i_{FB} = \begin{pmatrix} 1 + \Delta_{0,0} & \Delta_{0,1} \\ \Delta_{1,0} & 1 + \Delta_{1,1} \end{pmatrix} i_{FB} \quad (6)$$

In which the linear relation between the feed back currents i_{fb} (see Fig 16 – upon integration, these currents directly yield the preamp output signals) and the ideal currents i^{Ramo}, as predicted by the Ramo theorem is slightly deviating from the unity

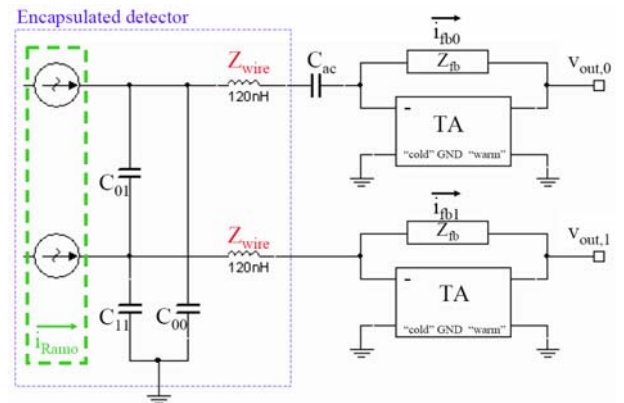matrix (for simplicity, only the relation between core and a single segment is shown)

Fig. 16 Simplified model of a single segmented detector network (where core channel is marked with "0" and for simplicity, only one of the 36 segments is shown)

The major impact has the AC coupling of the core preamplifier, which causes cross talk of the order of $\Delta_{i,0} = C_{0,i} / C_{ac}$: the core to segment capacity (~1pF, see table 3) divided by the core ac coupling capacity (1nF). (The other cross talk matrix elements are predicted negligible by this model as the much larger Miller equivalent capacity is replacing C_{ac} for DC coupled segments.)

Such cross talk matrix elements are routinely measured using a set of 10 DGF-4C CAMAC modules developed by XIA LLC for the MINIBALL detector array [2].
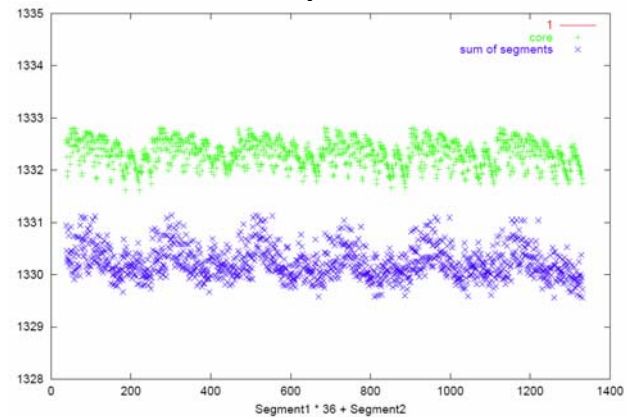

Fig.17 Cross talk measurement, energy shift for core and energy shifts for segments in all 2- fold hits (36x36 combinations)

By gating on 2-fold hits, energy shifts are observed in the segments as a function of hit pattern (presented in Fig.17 for all 36x36 combinations). As described in [9], it is the periodic variation in the capacities $C_{0,i}$ which finally leaves a finger print on the observed energy deficit in segment 2-folds. (In the core 2-folds, also electron trapping

mixes in).

3.4 Full Transfer function

The transfer function is frequency independent only in the low frequency range (< 1MHz). At higher frequencies, the true impedances of the wiring between detector and preamps play an increasing role. As the strategies in wiring are cryostat dependent, we cannot derive absolute expressions for their influence. We will limit the discussion therefore only to an idealized case where only the wire impedance between segments and preamps are modeled with a finite inductivity (see Fig. 16). (Individual cryostat wiring philosophies solutions differ in the treatment how "cold" ground and "warm" grounds are connected)

Within this model, the transfer function extends to:

$$i_{FB} = \mathbf{Z}^{-1} i_{Ramo} \cong$$

$$\underbrace{\frac{1}{\det(Z)}}_{\substack{\sim 1 \text{ below}\\ \text{resonance}}} \left[\underbrace{\begin{pmatrix} 1-\Delta_{0,0} & -\Delta_{0,1} \\ -\Delta_{1,0} & 1-\Delta_{1,1} \end{pmatrix}}_{\text{Low frequency solution}} + \underbrace{s Z_{wire} \begin{pmatrix} C_{0,0} & -C_{0,1} \\ -C_{1,0} & C_{1,1} \end{pmatrix}}_{\substack{\text{Extra term at high frequencies}\\ \text{(wiring dependent)}}} \right] i_{Ramo} \tag{7}$$

The impedance of a wire can be estimated as [10]:

$$L_{wire} = \frac{\mu l}{2\pi} \left(\ln\left(\frac{2l}{r_0}\right) - 1 \right) \tag{8}$$

As characteristic wire length, the crystal length was chosen (9cm) and a wire radius of 75μm. The frequency dependence of the four matrix elements in the transfer matrix $\mathbf{Z^{-1}}$ for the electronic scheme Fig 16 has been calculated as function of frequency in Fig 18. Below 1MHz, the solution is not influenced by the wire impedance. Traditional detectors, not requiring position sensitivity, can therefore be made insensitive to cryostat wiring.
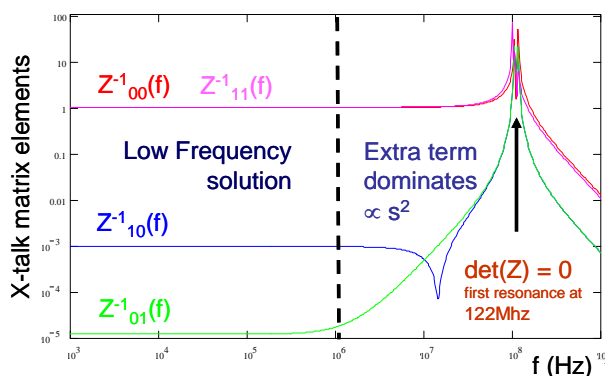
bandwidth above 1Mhz is requested for PSA. In this region, the cross talk is increasing with s^2, till finally the determinant of $\mathbf{Z}$ becomes zero and the system is fully resonant. This has often been observed in reality as well. For AGATA, typical resonances were observed at around 100Mhz, which is close to the value of 122Mhz predicted by the model with 120nH.

It is thus proven that the measured signals – depending on cryostat wiring strategy – differ from the ideal currents as predicted by the Ramo theorem. Again the pulser input on the core preamplifier becomes irreplaceable to measure the true transfer functions of the front-end electronics.

3.5 Frequency compensation

The reasons for frequency compensation of the charge sensitive loop equivalent operational amplifier are: noise reduction, flat amplitude response and obtaining highest bandwidth possible consistent with the pulse response requirements. [12]-[14] The implemented frequency compensating circuits are three fold, namely: two high-pass filters (as the Miller effect like internal compensations of the equivalent operational amplifiers), one lead-lag filter and one dominant-pole compensation circuit. As shown in Fig.19, the passive and active electronic components of the equivalent operation amplifier and its feedback loop are spread inside and outside the cryostat, but all compensating circuits are placed only outside the cryostat (i.e. in its warm part). The lead-lag compensation $R_1 * C_1 \approx (3-5)*10^{-9} s$ is rather high frequency compensation without sacrificing the close-loop gain performance.

Fig.18 Real transfer function with cryostat wiring and no external frequency compensation

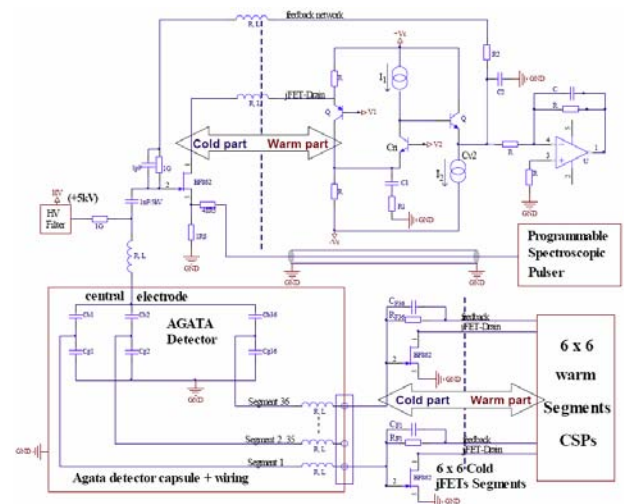When position sensitivity is demanded, also the

Fig.19 Front-end electronics and wiring layout of a 36-fold segmented and encapsulated HP-Ge detector in a single AGATA test cryostat

The dominant pole compensation compensates the pole existing in the more complex core feedback network shown in Fig.20.
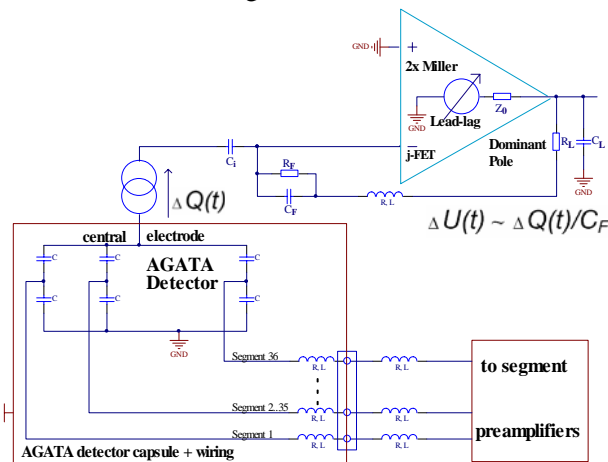

Fig.20 Simplified block diagram of the equivalent transimpedance amplifier and its frequency compensation network

We took advantage of the very large open loop gain of the charge sensitive stage and its quite small output impedance (Z_o) capable to drive the rather large output capacitor (C_L) of 15-27 pF. The R_L,C_L network acts efficiently as a dominant pole compensation without causing instabilities in interaction with the intrinsic equivalent operational amplifier pole: $R_L * C_L \approx (1-1.5)*10^{-9}\,s$

The transfer function and the Bode plot of the equivalent circuit shown in Fig.20 looks like that shown in Fig. 21. When the pole introduced by Z_o and C_L moves towards the zero frequency axis it comes close to τ_2 pole and it adds phase shift to the system. The increased phase shift increases peaking and decreases stability. Assuming that $Z_o \ll Z_F$, the closed-loop transfer function can be calculated simply by including C_L in the enclosed feedback loop.
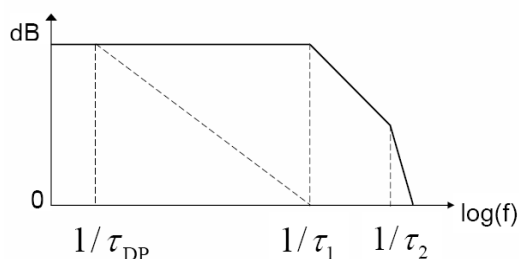

Fig. 21 Equivalent transfer function and Bode plot of the distributed equivalent transimpedance amplifier

As long as the equivalent operational amplifier has enough compliance and current to drive the

capacitive load and Z_o is small, the circuit functions as though the capacitor was not there. Thus we got the highest possible bandwidth consistent with the pulse response requirements given by the fast electron collection time at the central electrode of a HP-Ge Detector.

4 Conclusion

A very low noise, very wide dynamic range with a very clean transfer function charge-sensitive pre-amplifier has been developed and tested to be used with a highly segmented and encapsulated HP-Ge detector in the frame of the AGATA project. Furthermore its wide spectroscopic range has been successfully extended by more than one order of magnitude, by switching (below the maximum of the ADC range) from the standard amplitude spectroscopic method to the new TOT technique. The disadvantage of a small gap in the conversion range has been eliminated by implementing a dual range AGATA core preamplifier. An excellent energy resolution over the whole range was achieved, about 1.1keV @ 59.5keV, 2.1keV @ 1.33MeV (pulse height analysis mode) and 0.21% @ 8.99MeV and less than 0.04% above 50 MeV (in Time over Threshold mode).

There are already some very interesting applications of these techniques developed for large array of segmented detectors, e.g. due to mentioned advances in manufacturing large and highly segmented HP-Ge detectors and related fast and high-precision front-end electronics and digital electronics, it is now possible to build efficient and high-resolution Compton cameras[15]. By employing gamma-ray tracking procedures it is possible to get position resolution of 0.5 mm at 122 keV without the use of a attenuating collimator.

References:

[1] J. Simpson, "The AGATA Project", EPS Euro Conference XIX Nuclear Physics Divisional Conference, Journal of Physics: Conference Series 41, 2006, 72-80

[2] J. Eberth, G. Pascovici, H.G. Thomas, N. Warr, D. Weisshaar et al. "Miniball: A Gamma-Ray Spectrometer with Position-Sensitive Ge Detector for Nuclear Structure Studies at REX-ISOLDE", AIP Conf. Proc., 2003, Vol. 656, pp 349-356

[3] A. Pullia, G. Pascovici, B. Cahan, D. Weisshaar, C. Boiano, R. Bassini, M. Petcu, F. Zocca, "The AGATA charge sensitive preamplifiers with built-in active reset and pulser", Nucl. Sci. Symp. Conf. Record, 2004 IEEE Vol 3, Issue, Oct. 2004, pp 1411-1414

[4] G. Pascovici et al., "Programmable Stretcher and 16 k Channels Portable MCA" , private communication

[5] F. Zocca, A. Pullia, D. Bazzacco, G. Pascovici, "Wide Dynamic Range Front-End Electronics for Gamma Spectroscopy with a HP-Ge crystal of AGATA", Nucl. Sci. Symp. Conf. Record, 2007 IEEE, Vol.1, pp 7-13

[6] E. Gatti, G. Padovini, V. Radeka, "Signal evaluation in multi electrode radiations detectors by means of a time depending weighting vector", Nucl. Instr. Meth. Vol. 193, 1982, pp 651-653

[7] E. Pellegrini et al, Electric charge motion, induced current, energy balance and noise, Phys.Rev.B Vol 34 Nr.8 (1986) pp 5921-5924

[8] A. Pullia, R. Isocrate, R. Venturelli, D. Bazzacco, R. Bassini, C. Boiano, "Characterization of HPGe-segmented detectors from noise measurements", IEEE Trans. Nucl. Sci., Vol 51, 2004, pp 3086-3089

[9] B. Bruyneel, P. Reiter, A. Wiens, J. Eberth, H. Hess, A. Linnemann, G. Pascovici, N. Warr, D. Weisshaar, "Crosstalk properties of 36-fold segmented symmetric hexagonal HP-Ge Detectors", Nucl. Instr. Meth., 2008, to be published

[10] F.W. Grover, "Inductance Calculations: Working Formulas and Tables", D. Van Nostrand Company, Inc., New York, 1946.

[11] A.Tangel, M.Yakut, M. Ayar, " An Auto Calibrator for TIQ Based Flash ADC Designs", Proceedings of the 6th WSEAS Intern. Conf. on CSECS'07, Cairo, Egipt, Dec 29-31, 2007,pp.47-52

[12] B. Kuo, F. Golnaraghi, "Automatic Control Systems", John Willey & Sons,Inc., 2003

[13] Anand Paul, A. Ebenezer Jeyakumar, P.N. Neelakatan, Power minimization strategy in MOS transistors using quasi floating gate, www.wseas.us/e-library/conferences/singapore, 2003/ 467-210.doc

[14] S.V. Zamyatim, S.A. Gaivoronskiy, "The assignment Systems of Control Systems with Interval Parameters", in "Systems Theory and applications", editors: N. Mastorakis et al., Proc. of the 11th WSEAS International Multiconference CSCC (Circuits; Systems, Communications, Computers), Vol 2, 2007, pp 411-415

[15] K.Vetter, M. Bursk, L. Mihailescu, " Gamma-ray Imaging with Position Sensitive HPGe detectors", Nuclear Instruments and Methods in Physics Research, Section A, 2004, vol.525, pp.322-327